Impacts of the 2015-2016 El Niño on the California Current System: Early assessment and comparison to past events

Michael G. Jacox[1,2], Elliott L. Hazen[2], Katherine D. Zaba[3], Daniel L. Rudnick[3], Christopher A. Edwards[4], Andrew M. Moore[4], and Steven J. Bograd[2]

[1]Institute of Marine Sciences, University of California, Santa Cruz, California, USA

[2]Environmental Research Division, Southwest Fisheries Science Center, NOAA, Monterey, California, USA

[3]Scripps Institution of Oceanography, La Jolla, California, USA

[4]Ocean Sciences Department, University of California, Santa Cruz, California, USA

Corresponding Author:

Michael G. Jacox, NOAA/NMFS, Southwest Fisheries Science Center, Environmental Research Division, 99 Pacific Street, Suite 255A, Monterey, CA 93940, USA

(mjacox@ucsc.edu)

Key Points

- Initial impacts of the 2015-16 El Niño on the CCS physical state are evaluated
- Local anomalies much weaker than expected based on tropical El Niño strength
- Relatively weak El Niño imprint occurs on backdrop of large multi-year anomalies

Abstract

The 2015-16 El Niño is one of the strongest on record, comparable to the 1982-83 and 1997-98 events that triggered widespread ecosystem change in the northeast Pacific. Here, we describe initial impacts of the 2015-16 El Niño on the California Current System (CCS), and place them in historical context using a data assimilative regional ocean model and autonomous glider observations. El Niño impacts on the physical state of the CCS are weaker than expected based on tropical SST anomalies; temperature and density fields reflect persistence of multi-year anomalies rather than an El Niño signature. We therefore anticipate effects of El Niño on spring/summer 2016 chlorophyll concentrations to be relatively weak, through productivity could still be suppressed if recent conditions persist. This study highlights the need for regional El Niño indices and demonstrates the potential to assess El Niño impacts before the upwelling season, when altered ecosystem functioning is most apparent.

1. Introduction

The 2015-16 El Niño continues a string of significant climate events in and around the north Pacific, following on the heels of an extreme drought that struck California beginning in 2012 [*Swain et al*., 2014; *Diffenbaugh et al*., 2015], large-scale anomalous warming of the northeast Pacific beginning in 2013 and reaching record high sea surface temperature (SST) in 2014-15 [*Bond et al*., 2015], and tropical warming in 2014 that hinted at the development of a major El Niño in winter 2014-15 [*Ludeschera et al.*, 2014], but failed to develop as expected [*McPhaden*, 2015]. In November 2015, the widely used Niño 3.4 index indicated the warmest tropical Pacific SST anomalies on record (Fig. 1), inviting speculation that this El Niño and associated storms could alleviate drought conditions in the western United States and break up the northeast Pacific warm anomaly. At the same time, comparisons with past El Niño events of similar magnitude suggest the potential for substantial marine ecosystem impacts in the California Current System (CCS). The 1997-98 El Niño, for example, was implicated in dramatic and widespread changes to the physical, chemical, and biological environments of the CCS [e.g., *Kahru and Mitchell*, 2000; *Bograd and Lynn*, 2001; *Chavez et al*., 2002a and references therein].

The imprint of El Niño on the CCS arrives through two mechanisms: (i) atmospheric teleconnection whereby tropical convection excites atmospheric Rossby waves that tend to strengthen the Aleutian Low and displace it to the southeast of its climatological position, reducing (increasing) the strength of upwelling (downwelling) favorable winds along the North American west coast [*Hoskins and Karoly*, 1981; *Alexander et al.*, 2002; *Schwing et al.*, 2002], and (ii) remote ocean forcing by equatorial and coastal Kelvin wave propagation from the tropics [*Enfield and Allen,* 1980; *Meyers et al.*, 1998; *Strub and James*, 2002], which depresses the

64 thermocline and nutricline in the CCS [*Huyer and Smith*, 1985; *Chavez et al.*, 2002b]. The
65 relative importance of these two mechanisms in determining the physical and biogeochemical
66 state of the CCS during El Niño has long been a subject of debate [e.g., *Simpson*, 1993 cf. *Huyer*
67 *and Smith*, 1985], however recent studies suggest that remote forcing dominates in the southern
68 CCS (south of Point Conception, ~34.5˚N), local atmospheric forcing dominates in the northern
69 CCS (north of Cape Mendocino, ~40.5˚N), and the two have comparable influence in the central
70 CCS [*Frischknecht et al.*, 2015; *Jacox et al.*, 2015a,b]. In this paper, we explore impacts of the
71 2015-16 El Niño on the CCS, placing current conditions in the context of widespread anomalies
72 in recent years as well as El Niño – Southern Oscillation (ENSO) variability over multiple
73 decades (e.g., the 1982-83 and 1997-98 El Niños). We examine physical oceanographic
74 conditions, particularly the subsurface density field, and use our findings to infer potential
75 bottom-up effects on productivity in the coming spring/summer off central and southern
76 California.
77
78 **2. Methods**
79 **2.1. Data**
80 **2.1.1. Temperature**
81 We use several products to document temperature anomalies in the equatorial Pacific (Fig. 1).
82 The Niño 3.4 Index (http://www.cpc.ncep.noaa.gov/data/indices/) is a measure of equatorial
83 Pacific SST anomalies based on monthly averaged data from the Extended Reconstructed Sea
84 Surface Temperature (ERSST) v4, using centered base periods to remove any long-term trends.
85 Subsurface temperature variability in the tropical Pacific is characterized using 20˚C isotherm
86 depth anomalies, averaged from 2˚S to 2˚N, from the Global Ocean Data Assimilation System

87 (GODAS, http://www.cpc.ncep.noaa.gov/products/GODAS/pentad.shtml). Surface temperature
88 anomalies in the CCS during the El Niños of 1982-83, 1997-98, and 2015-16 are compared using
89 version 2 of NOAA's 0.25˚ optimum interpolation SST product (OISST.v2) [*Reynolds et al.,*
90 2007].
91
92 **2.1.2. Chlorophyll**
93 Surface chlorophyll estimates for 1998-2015 are from the merged 4 km resolution CCS dataset
94 described by Kahru et al. [2012, 2015]. This product utilizes >12,000 in situ measurements to
95 regionally optimize surface chlorophyll algorithms for each of five satellite ocean color sensors
96 (OCTS, SeaWiFS, MERIS, MODIS-A, and VIIRS). Daily remote sensing reflectance
97 measurements are used to produce chlorophyll estimates for each sensor. Those chlorophyll
98 estimates are then merged, minimizing differences with observations as well as differences
99 between sensors during overlapping time periods.
100
101 **2.1.3. Underwater Gliders**
102 Since late 2006, Spray gliders [Sherman et al., 2001; Rudnick et al., 2004] have continuously
103 occupied lines 66.7, 80, and 90 of the California Cooperative Oceanic Fisheries Investigations
104 (CalCOFI) sampling grid (Fig. 3). Each glider line extends 350-500 km offshore, takes 2-3
105 weeks to complete, and consists of continuous vertical profiles from the surface to 500 m depth
106 covering ~3 km in the along-track direction. Glider data are objectively mapped to three-
107 dimensional grids with horizontal, vertical, and temporal resolutions of 5 km, 10 m, and 10 days,
108 respectively, using the method of *Bretherton et al.* [1976]. The mapping algorithm uses

109 horizontal and temporal decorrelation scales of 30 km and 60 days, respectively, which are
110 intended to filter out high frequency variability [*Rudnick and Cole*, 2011].
111
112 **2.2. Ocean Model**
113 We employ a 31-year (1980-2010) regional ocean reanalysis to provide historical context for
114 impacts of ENSO variability on the CCS. This reanalysis uses the Regional Ocean Modeling
115 System (ROMS) with 4-Dimensional Variational (4D-Var) data assimilation and is described in
116 detail elsewhere [*Neveu et al*., 2016], so we provide only a brief overview here. The model
117 domain covers the North American west coast from 30 to 48˚N and from 115.5 to 134˚W, with
118 0.1˚ horizontal resolution and 42 terrain-following vertical levels. Surface forcing derives from a
119 combination of the European Centre for Medium-range Weather Forecasting 40-year (ERA-40)
120 [*Uppala et al.,* 2005] and Interim (ERA Interim) [*Dee et al.,* 2011] reanalyses and the Cross-
121 Calibrated Multi Platform (CCMP) wind product [*Atlas et al.*, 2011]. Conditions at the lateral
122 boundaries are provided by the Simple Ocean Data Assimilation (SODA) reanalysis [*Carton and*
123 *Giese*, 2008]. Assimilated data include satellite SST from the Advanced Very High Resolution
124 Radiometer (AVHRR), Moderate Resolution Imaging Spectroradiometer (MODIS), and
125 Advanced Microwave Scanning Radiometer-EOS (AMSR-E), satellite SSH from Archiving,
126 Validation, and Interpretation of Satellite Oceanographic data (AVISO), and *in situ* hydrographic
127 data from version 2a of the quality controlled ENSEMBLES database maintained by the U.K.
128 Met Office [*Ingleby and Huddleston*, 2007]. In previous studies, this reanalysis and a similar
129 configuration without data assimilation have been used to investigate physical and
130 biogeochemical dynamics off the US west coast, including ENSO-driven variability [*Jacox et*
131 *al.*, 2014; 2015a,b].

132

133 **2.3. Merging Model and Glider Data**

134 The data sources described in the previous two sections, the underwater glider network off
135 central and southern California and a historical reanalysis of the CCS, cover the periods 2007-
136 present and 1980-2010, respectively. Here, we merge these two datasets to develop time series
137 extending from 1980-present, providing historical context for the conditions accompanying the
138 2015-16 El Niño. We do not attempt to fully merge the modeled and glider-based ocean state
139 estimates. Rather, we focus on a key derived variable, the depth of the 26.0 kg m^{-3} potential
140 density isopycnal ($d_{26.0}$), a proxy for pycnocline depth that is closely tied to nutrient supply and
141 resultant productivity, and can be modulated by local upwelling [*Lynn et al.,* 2003], remote (e.g.,
142 ENSO-related) forcing [*Jacox et al.,* 2015a], and regional influences [e.g., anomalous northeast
143 Pacific warming in 2014-15; *Zaba and Rudnick*, 2015]. For each of the three cross-shore glider
144 transects, we compute monthly mean $d_{26.0}$ and average across a 50 km coastal band, which is
145 chosen to reflect the region of greatest influence by coastal waves and anomalous upwelling
146 associated with El Niño. Model-based estimates of $d_{26.0}$ are similarly averaged in time and space,
147 using grid cells that overlap glider tracks. Model and glider-based estimates of $d_{26.0}$ are shown in
148 Fig. 3 for the 4-year period (2007-2010) in which they overlap. While model estimates of $d_{26.0}$
149 are strongly correlated with glider estimates ($r = 0.75 – 0.87$, Fig. S1), they are generally too
150 deep and underestimate the observed variance, consistent with a known warm bias and
151 underestimation of salinity variability at typical pycnocline depths in the model [*Neveu et al.*,
152 2016]. We therefore use 2007-2010 data to bias-correct and scale model estimates of $d_{26.0}$ on
153 each line such that they match the mean and variance of glider estimates for the overlapping

154 period (Fig. 3). The corrected model estimates are then combined with glider estimates to
155 produce consistent time series of $d_{26.0}$ extending from 1981 to early 2016 (Fig. 4).
156
157 **3. Tropical Pacific Temperature Anomalies**
158 The evolution of El Niño strength, as measured by the Niño 3.4 Index, is shown in Fig. 1a for
159 each event since 1950. While tropical SST anomalies consistently peak in late fall or winter,
160 individual events evolve differently in the years preceding and following their peaks. The 1997-
161 98 El Niño was notable not only for its maximum magnitude, but also for dramatic transitions
162 out of the cool conditions of 1996-97 and into a strong La Niña beginning in late 1998. In
163 contrast, the tropical Pacific was already anomalously warm prior to the ramp-up of the 2015-16
164 El Niño, owing to an aborted El Niño the year prior [*McPhaden*, 2015]. While the Niño 3.4
165 Index reached nearly identical maximal values in November 1997 and November 2015 (2.32˚C
166 vs. 2.36˚C), the net warming in the year preceding the 1997 peak (i.e., from November 1996 to
167 November 1997) was a full degree higher than in the year preceding the 2015 peak (2.68˚C vs.
168 1.62˚C). For comparison, the peak tropical SST anomaly in the 1982-83 El Niño was slightly
169 lower than that seen in 1997-98 or 2015-16 (2.21˚C), but the warming in the preceding year was
170 closer to that seen in 1997 (2.29˚C).
171
172 In the subsurface, the 20˚C isotherm depth (d_{20C}) tracks tropical Pacific Kelvin wave generation.
173 During the 1982-83 and 1997-98 El Niños, there is a clear eastward propagation of d_{20C}
174 anomalies, with a pronounced east-west dipole and eastern equatorial d_{20C} anomalies >50 m
175 persisting from October through at least February (Fig. 1b). While surface SST anomalies in
176 2015-16 suggest an event similar in magnitude to the strongest El Niños on record, the evolution

177 of d_{20C} has been in stark contrast to those events. Tropical Pacific d_{20C} anomalies changed little
178 throughout 2015 and into 2016, with a persistent and relatively weak east-west dipole that
179 appears to reflect persistence of existing anomalies rather than a building El Niño.
180
181 **4. Development of the 2015-16 El Niño in the CCS Relative to Past Events**
182 Tropical subsurface anomaly patterns during the 2015-16 El Niño, and their departure from those
183 seen during significant past events, are mirrored in the CCS. During the winters of 1982-83 and
184 1997-98, surface temperature anomalies were greatest near shore, consistent with the influence
185 of coastally trapped waves propagating from the topics and anomalously weak upwelling (Fig.
186 2). During the 2015-16 El Niño, however, no such cross-shore structure was evident. Rather,
187 anomalously warm surface temperatures were spatially uniformly distributed, more consistent
188 with ongoing decay of the northeast Pacific warm anomaly that reached the US west coast in
189 spring/summer 2014 [*Bond et al*., 2015] than with a warming signature of El Niño. The
190 subsurface tells a similar story; anomalies in the 26.0 kg m^{-3} isopycnal depth ($d_{26.0}$) were already
191 established by mid-2014 [*Zaba and Rudnick*, 2016] and remained nearly constant through late
192 2015 into 2016 (Fig. 4). In contrast, past strong El Niños were characterized by a dramatic
193 deepening of $d_{26.0}$ in the latter half of the year, with anomalies peaking in December/January, 1-2
194 months after peak tropical SST anomalies (Fig. 4). While our 35-year time series suggest that the
195 Niño 3.4 index is generally a good proxy for wintertime $d_{26.0}$ off central and southern California
196 ($r = 0.75$-0.83, Fig. 5), the three strongest El Niños are all significant outliers. Pycnocline depths
197 in 1982-83 ranged from ~0.5-2 standard deviations (σ) deeper than those predicted by Niño 3.4
198 based on 1981-2015 data. On all three glider lines, $d_{26.0}$ in 1997-98 was ~2σ deeper than that
199 predicted by Niño 3.4. In contrast, $d_{26.0}$ in the winter of 2015-16 was ~1σ shallower than that

200 predicted by the Niño 3.4 anomaly (Fig. 4), again highlighting the relatively weak expression of
201 this particular El Niño in the CCS.
202
203 **5. Impacts on Primary Production in the Central and Southern CCS**
204 The 1982-83 and 1997-98 El Niños were both followed by sharp reductions in spring/summer
205 phytoplankton biomass off the California coast [*Fiedler*, 1984; *Kahru and Mitchell*, 2000]. These
206 reductions were attributed to weak upwelling and/or a deep pycnocline/nutricline, each of which
207 decreases nutrient supply to the surface mixed layer. Here, we explore the relationship between
208 mid-winter (December-February) $d_{26.0}$ variability and biological impacts the following
209 spring/summer (April-July) using an Empirical Orthogonal Function (EOF) decomposition of the
210 surface chlorophyll field from 30˚ to 40˚N and from the coast to 300 km offshore. The first EOF
211 has little spatial structure south of San Francisco Bay (~38˚N), capturing broad-scale interannual
212 variability in spring/summer chlorophyll concentrations. EOF1 explains 32% of the observed
213 variance, and is significantly negatively correlated with $d_{26.0}$ on all three glider lines ($r \approx -0.7$,
214 Fig. 6), suggesting that the physical ocean state in winter is a useful leading indicator of
215 upwelling season productivity. Interestingly, the correlation between EOF1 and the Niño 3.4
216 Index is much weaker ($r = -0.53$), further demonstrating the limitations of projecting El Niño
217 impacts on the CCS from tropical SST anomalies alone. Note that the lower modes of
218 chlorophyll variability (EOF2, 11% explained variance; EOF3, 10% explained variance) describe
219 spatially heterogeneous fluctuations and are not strongly correlated with $d_{26.0}$ ($r = 0.14$-0.27) or
220 Niño 3.4 ($r = 0.11$-0.13). Based solely on $d_{26.0}$ in winter 2015-16 and the linear fits in Fig. 6,
221 spring/summer 2016 chlorophyll anomalies off central and southern California should be
222 negative, but of far smaller magnitude than those seen in 1998. However, in the past two years,

223 unprecedented warming of the northeast Pacific brought strongly negative chlorophyll anomalies
224 (Fig. 6), as well as dramatic impacts on species abundance and distribution throughout the
225 marine food web [*Bond et al.*, 2015; *Peterson et al.*, 2016]. We can therefore envision scenarios
226 for spring/summer 2016 where (i) the background ocean state returns to something near the
227 climatological mean, and surface chlorophyll anomalies are much smaller than they were in 1998
228 (blue dot in Fig. 6), or (ii) the impact of multi-year anomalous conditions persists, and while El
229 Niño is not the primary cause, chlorophyll levels are comparable to those seen in 1998 (lower
230 blue error bar in Fig. 6).
231
232 **6. Conclusion**
233 We have shown here the initial physical oceanographic response of the California Current
234 System to the 2015-2016 El Niño. While tropical Pacific SST anomalies reached record highs in
235 late 2015, they did not translate to strong equatorial Kelvin wave generation, as evidenced by
236 relatively small perturbations to subsurface isotherms. The subsurface response in the central and
237 southern CCS was similarly weak, especially when compared to the 1982-83 and 1997-98 El
238 Niños. We therefore expect the direct impacts of the 2015-16 El Niño on primary production in
239 the CCS to be weaker than in the 1982-83 or 1997-98 El Niños, however it is important to note
240 that the 2015-16 El Niño is occuring on a backdrop of multi-year highly anomalous conditions
241 that have drastically impacted the ecosystem already. ENSO events come in many flavors
242 [*Capotondi et al.*, 2015], and the disparity in CCS responses to El Niño events of similar
243 magnitude (based on widely used indices) highlights the need for more holistic metrics of ENSO
244 events and/or regional metrics of their effects. Our study shows one such example ($d_{26.0}$), which
245 correlates strongly with ENSO indices but is a much better predictor of biological impacts. Our

246 study reflects technological advances that now enable near real time assessment of an ongoing El
247 Niño, particularly its regional impacts in the context of historical variability, based on the best
248 available data from ocean models, satellites, and autonomous platforms.
249
250 **Acknowledgments**
251 This work was supported by funding from NSF grant #OCE1061434 and NOAA's Integrated
252 Ecosystem Assessment program. The California Underwater Glider Network is supported by the
253 NOAA Climate Observations Division and the Southern California Coastal Ocean Observing
254 System. Model output from the ROMS historical reanalysis can be obtained from
255 oceanmodeling.ucsc.edu.
256
257 **References**
258 Alexander, M. A., I. Bladé, M. Newman, J. R. Lanzante, N. C. Lau, and J. D. Scott (2002),
259 The atmospheric bridge: The influence of ENSO teleconnections on air-sea interaction over the
260 global oceans, *J. Clim.*, *15*(16), 2205-2231.
261 Atlas, R., R. N. Hoffman, J. Ardizzone, S. M. Leidner, J. C. Jusem, D. K. Smith, and D.
262 Gombos (2011), A cross-calibrated, multiplatform ocean surface wind velocity product for
263 meteorological and oceanographic applications, *Bull. Am. Meteorol. Soc.*, *92*, 157–174,
264 doi:10.1175/2010BAMS2946.1.
265 Bograd, S. J., and R. J. Lynn (2001), Physical-biological coupling in the California Current
266 during the 1997–99 El Niño-La Niña cycle, *Geophys. Res. Lett*., 28, 275–278,
267 doi:10.1029/2000GL012047.
268 Bond, N. A., M. F. Cronin, H. Freeland, and N. Mantua (2015), Causes and impacts of the

2014 warm anomaly in the NE Pacific. *Geophys. Res. Lett.*, *42*(9), 3414-3420.

Bretherton, F. P., R. E. Davis, and C. B. Fandry (1976), Technique for objective analysis and design of oceanographic experiments applied to MODE-73, Deep-Sea Res., 23(7), 559–582, doi:10.1016/0011-7471(76)90001-2.

Capotondi, A., et al. (2015), Understanding ENSO diversity, *Bull. Am. Meteorol. Soc.,* 96(6), 921-938.

Carton, J.A., and B. S. Giese (2008), A reanalysis of ocean climate using simple ocean data assimilation (SODA), *Mon. Wea. Rev*., 136, 2999–3017.

Chavez, F. P., Collins, C. A., Huyer, A., & Mackas, D. L. (2002a). El Niño along the west coast of North America. *Prog. Oceanogr.*, *54*(1), 1-5.

Chavez, F., J. Pennington, C. Castro, J. Ryan, R. Michisaki, B. Schlining, P. Walz, K. Buck, A. McFadyen, and C. Collins (2002b), Biological and chemical consequences of the 1997–1998 El Niño in central California waters, *Prog. Oceanogr.*, 54(1-4), 205–232, doi:10.1016/S0079-6611(02)00050-2.

Dee, D. P., et al. (2011), The ERA-Interim reanalysis: Configuration and performance of the data assimilation system, *Q. J. R. Meteorol. Soc.*, 137, 553–597.

Diffenbaugh, N. S., D. L. Swain, and D. Touma (2015), Anthropogenic warming has increased drought risk in California, *Proc. Nat. Acad. Sci.*, *112*(13), 3931-3936.

Doyle, J.D., Q. Jiang, Y. Chao, and J. Farrara (2009), High-resolution atmospheric modeling over the Monterey Bay during AOSN II, *Deep Sea Res. II*, 56, 87–99.

Enfield, D., and J. Allen (1980), On the structure and dynamics of monthly mean sea-level anomalies along the Pacific coast of North and South-America, *J. Phys. Oceanogr.*, 10(4), 557–578, doi:10.1175/1520-0485(1980)0102.0.CO;2.

Fiedler, P. C. (1984), Satellite observations of the 1982-1983 El Niño along the US Pacific coast, *Science*, *224*(4654), 1251-1254.

Frischknecht, M., M. Münnich, and N. Gruber (2015), Remote versus local influence of ENSO on the California Current System, *J. Geophys. Res.*, 120, 1353–1374, doi:10.1002/2014JC010531.

Hoskins, B. J., and D. J. Karoly (1981), The steady linear response of a spherical atmosphere to thermal and orographic forcing, *J. Atmos. Sci.*, *38*(6), 1179-1196.

Huyer, A., and R. L. Smith (1985), The signature of El Niño off Oregon, 1982–1983, *J. Geophys. Res.*, 90, 7133–7142.

Ingleby, B., and M. Huddleston (2007), Quality control of ocean temperature and salinity profiles - Historical and real-time data, *J. Mar. Syst.*, *65*, 158–175.

Jacox, M. G., A. M. Moore, C. A. Edwards, and J. Fiechter (2014), Spatially resolved upwelling in the California Current System and its connections to climate variability, *Geophys. Res. Lett.*, 41, 3189–3196, doi:10.1002/2014GL059589.

Jacox, M. G., J. Fiechter, A. M. Moore, and C. A. Edwards (2015a), ENSO and the California Current coastal upwelling response, *J. Geophys. Res*., 120, 1691–1702, doi:10.1002/2014JC010650.

Jacox, M. G., S. J. Bograd, E. L. Hazen, and J. Fiechter (2015b). Sensitivity of the California Current nutrient supply to wind, heat, and remote ocean forcing. *Geophys. Res. Lett.*, *42*(14), 5950-5957.

Kahru, M., and B. G. Mitchell (2000), Influence of the 1997–98 El Nino on the surface chlorophyll in the California Current, *Geophys. Res. Lett.*, *27*(18), 2937-2940.

Kahru, M., R. M. Kudela, M. Manzano-Sarabia, and B. G. Mitchell (2012), Trends in the surface chlorophyll of the California Current: Merging data from multiple ocean color satellites, *Deep Sea Res. Part II,* 77-80, 89-98.

Kahru, M., R. M. Kudela, C. R. Anderson, and B. G. Mitchell (2015), Optimized merger of ocean color algorithms, *IEEE Geosci. Rem. Sens. Lett.*, 12(11), 2282-2285.

Ludeschera, J., A. Gozolchianib, M. I. Bogacheva, A. Bundea, S. Havlin, and H. J. Schellnhuberd (2014), Very early warning of next El Niño, *Proc. Natl. Acad. Sci. U.S.A.*, 111(6), 2064–2066, doi:10.1073/pnas.1323058111.

Lynn, R. J., S. J. Bograd, T. K. Chereskin, and A. Huyer (2003), Seasonal renewal of the California Current: The spring transition off California, J. Geophys. Res., 108(C8), 3279, doi:10.1029/2003JC001787.

McPhaden, M. J. (2015), Playing hide and seek with El Niño, *Nat. Clim. Chang.,* 5, 791-795.

Meyers, S. D., A. Melsom, G. T. Mitchum, and J. J. O'Brien (1998), Detection of the fast Kelvin wave teleconnection due to El Niño-Southern Oscillation, *J. Geophys. Res*., 103(C12), 27,655–27,663, doi:10.1029/98JC02402.

Neveu, E., et al. (2016) An historical analysis of the California Current circulation using ROMS 4D-Var. Part I: System configuration and diagnostics, *Ocean Modell*.

Peterson, W., N. Bond, and M. Robert (2016), The Blob (Part Three): Going, going, gone?, *PICES Press*, 24(1), 46-48.

Reynolds, R.W., T. M. Smith, C. Liu, D. B. Chelton, K. S. Casey, and M. G. Schlax (2007), Daily high-resolution-blended analyses for sea surface temperature, *J. Clim*., 20, 5473–5496.

Rudnick, D. L., and S. T. Cole (2011), On sampling the ocean using underwater gliders, J. Geophys. Res., 116, C08010, doi:10.1029/2010JC006849.

Rudnick, D. L., R. E. Davis, C. C. Eriksen, D. M. Fratantoni, and M. J. Perry (2004), Underwater gliders for ocean research, Mar. Technol. Soc. J., 38(2), 73–84.

Schwing, F., T. Murphree, L. DeWitt, and P. Green (2002), The evolution of oceanic and atmospheric anomalies in the northeast Pacific during the El Niño and La Niña events of 1995–2001, *Prog. Oceanogr.*, 54(1–4), 459–491, doi:10.1016/S0079-6611(02)00064-2.

Sherman, J., R. E. Davis, W. B. Owens, and J. Valdes (2001), The autonomous underwater glider "Spray", IEEE J. Oceanic Eng., 26(4), 437–446.

Simpson, J. J. (1983), Large-scale thermal anomalies in the California Current during the 1982–1983 El Niño, *Geophys. Res. Lett.*, 10, 937– 940, doi:10.1029/GL010i010p00937.

Strub, P., and C. James (2002), The 1997–1998 oceanic El Niño signal along the southeast and northeast Pacific boundaries—An altimetric view, *Prog. Oceanogr.*, 54(1–4), 439–458, doi:10.1016/S0079-6611(02)00063-0.

Swain, D. L., M. Tsiang, M. Haugen, D. Singh, A. Charland, B. Rajaratnam, and N. S. Diffenbaugh (2014), The extraordinary California drought of 2013/2014: Character, context, and the role of climate change, *Bull. Am. Meteorol. Soc*., *95*(9), S3.

Uppala, S. M., et al. (2005), The ERA-40 re-analysis, Q. J. R. Meteorol. Soc., 131, 2961–3012.

Zaba, K. D., and D. L. Rudnick (2016), The 2014–2015 warming anomaly in the Southern California Current System observed by underwater gliders, *Geophys. Res. Lett.*, 43, doi:10.1002/2015GL067550.

Figures

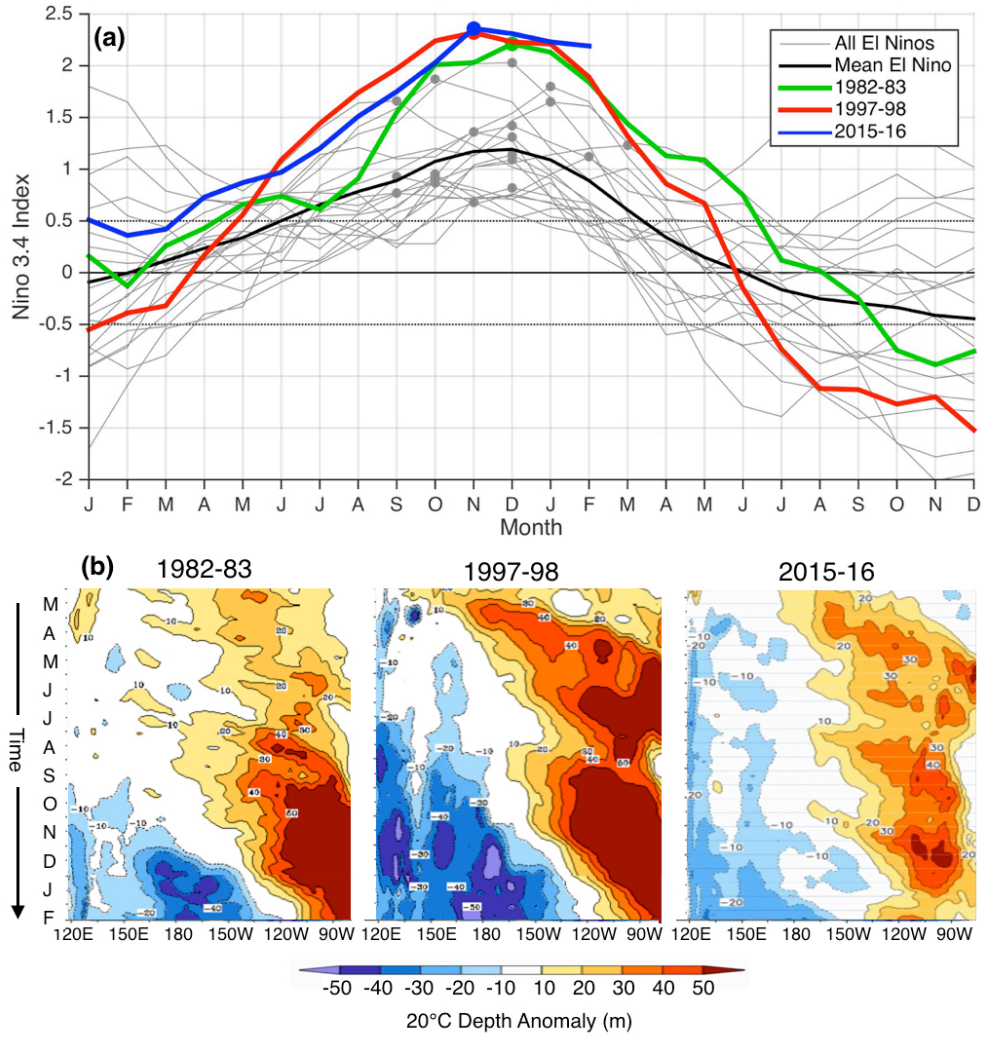

Figure 1: Surface and subsurface evolution of the equatorial Pacific temperature field during El Niño events. (a) Two-year progression of the Niño 3.4 Index for each El Niño since 1950. Circles indicate peak Niño 3.4 amplitude for each event. Dotted lines mark thresholds used to define El Niño and La Niña events. (b) Hovmöller plots of 20˚C isotherm depth anomalies across the equatorial Pacific, averaged from 2˚S to 2˚N, for March to February of 1982-83, 1997-98, and 2015-16 (note time progresses from top to bottom). Panel (b) was adapted from http://www.cpc.ncep.noaa.gov/products/GODAS/pentad.shtml.

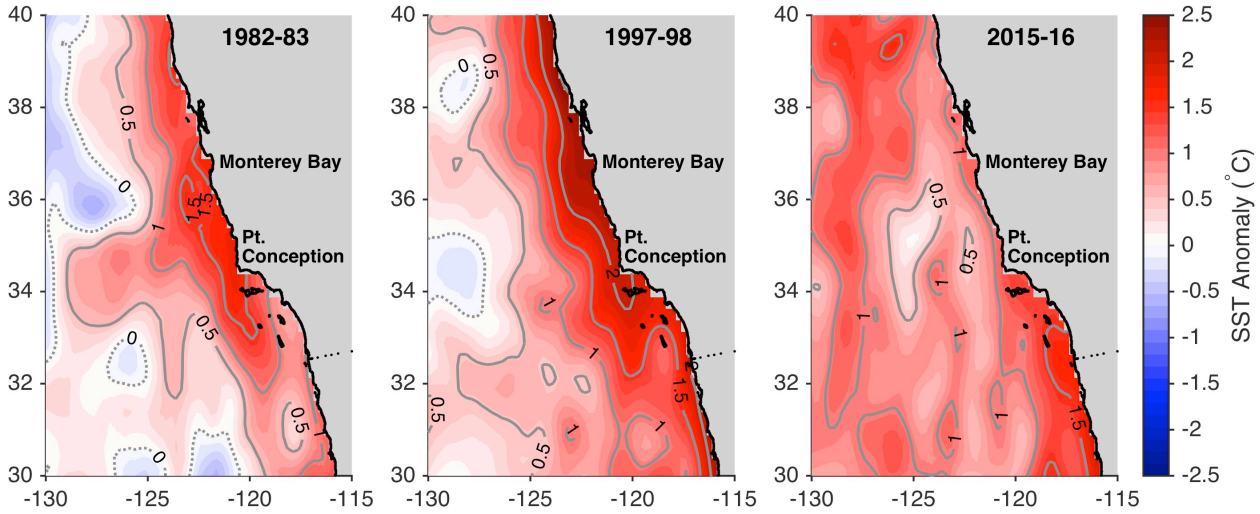

Figure 2: December-February mean SST anomalies for the winters of 1982-83, 1997-98, and 2015-16, from NOAA's 0.25˚ Optimal Interpolation SST (OISST) product.

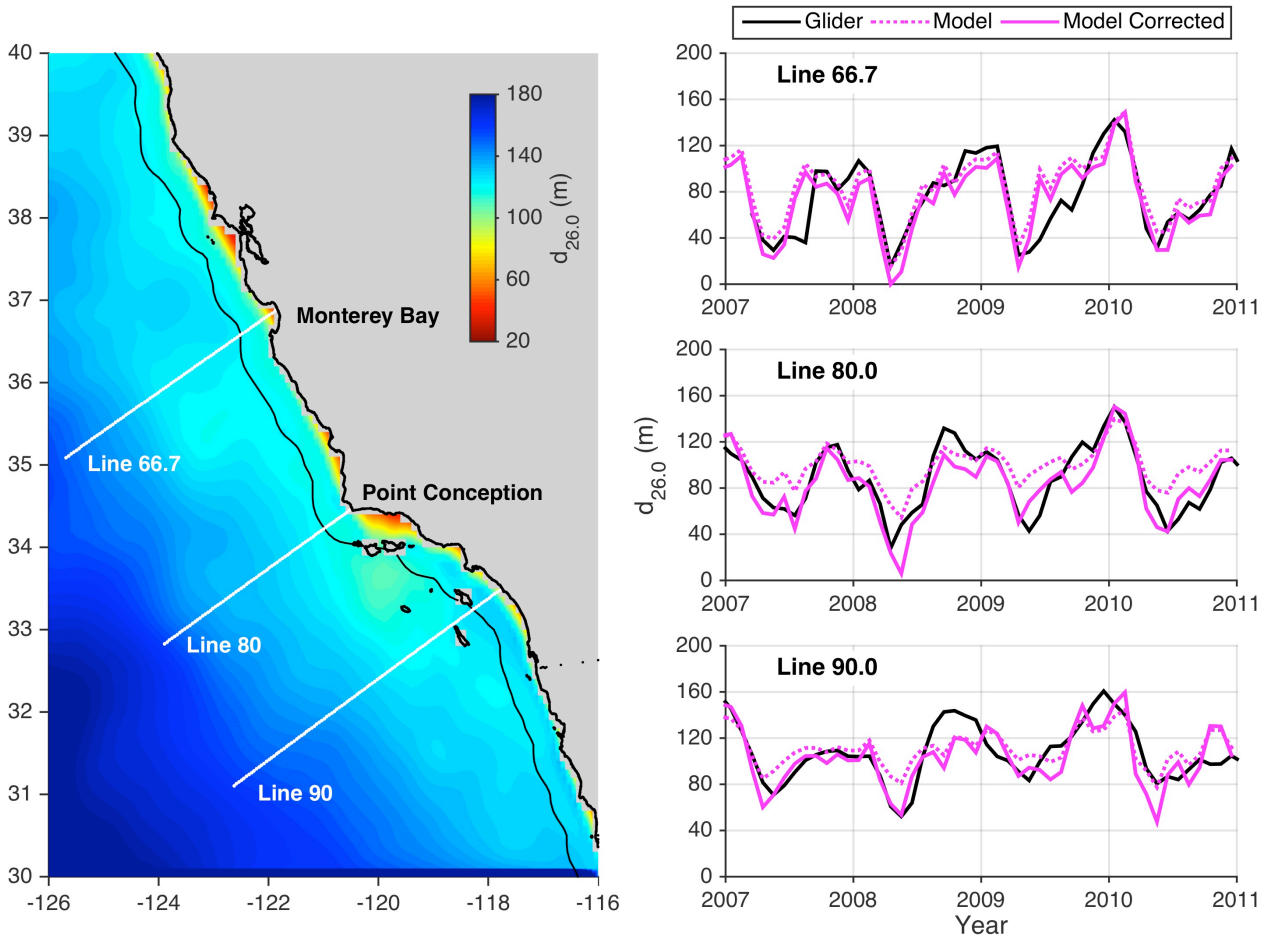

Figure 3: (left) December-February mean depth of the 26.0 kg m^{-3} isopycnal ($d_{26.0}$), computed from the ROMS reanalysis for the years 1981-2010. White lines are nominal positions of glider tracks and a black contour marks 50 km from shore. (right) Glider and ROMS estimates of $d_{26.0}$ for the overlapping period. Isopycnal depths were averaged within 50 km of the coast. The corrected model time series has the same mean and variance as the glider data (Section 2.3).

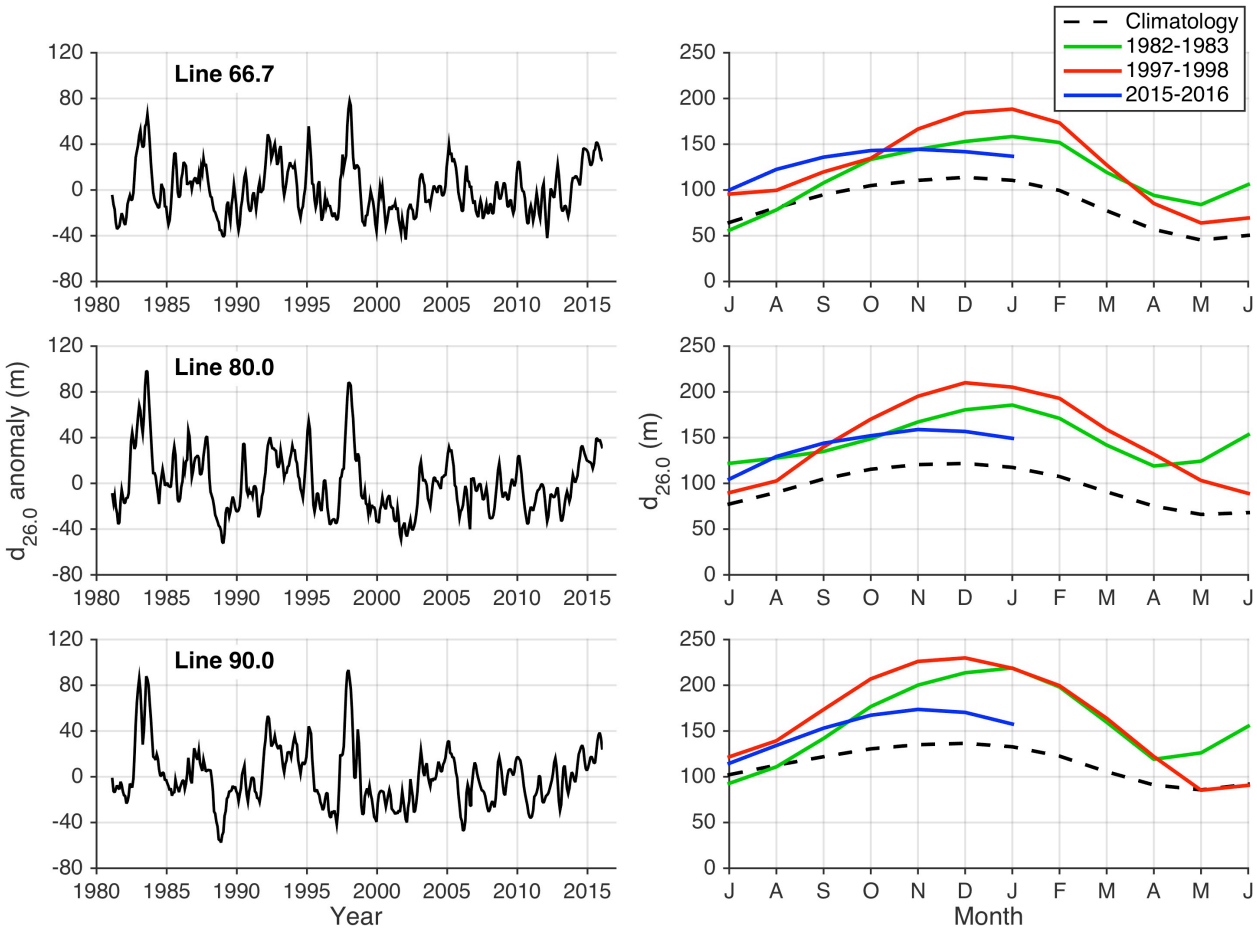

Figure 4: (left) Jan. 1981 – Feb. 2016 time series of $d_{26.0}$ anomalies from the merged model-glider data. (right) 12-month (July-June) evolution of $d_{26.0}$ during the 1982-83, 1997-98, and 2015-16 El Niños, as compared to the 1981-2015 climatology. All time series are smoothed with a 3-month running mean.

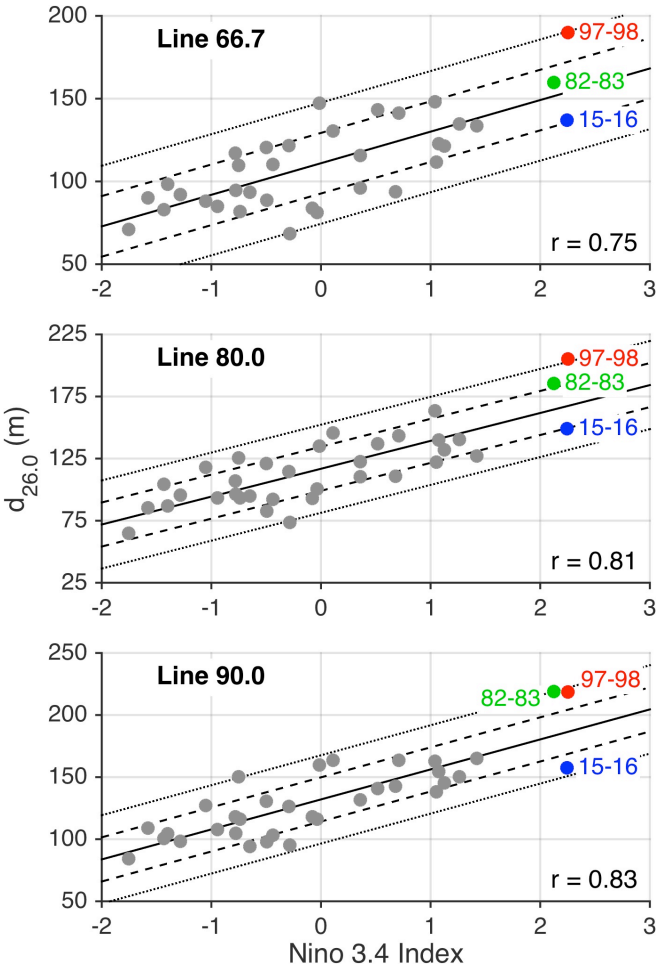

Figure 5: December-February mean $d_{26.0}$ (from merged model-glider data) plotted against November-January mean Niño 3.4 anomalies for each winter from 1981-82 to 2015-16. Isopycnal depths are averaged within 50 km of shore. Solid lines are linear fits to the data, dashed and dotted lines are ±1 and ±2 standard deviations from the linear fit.

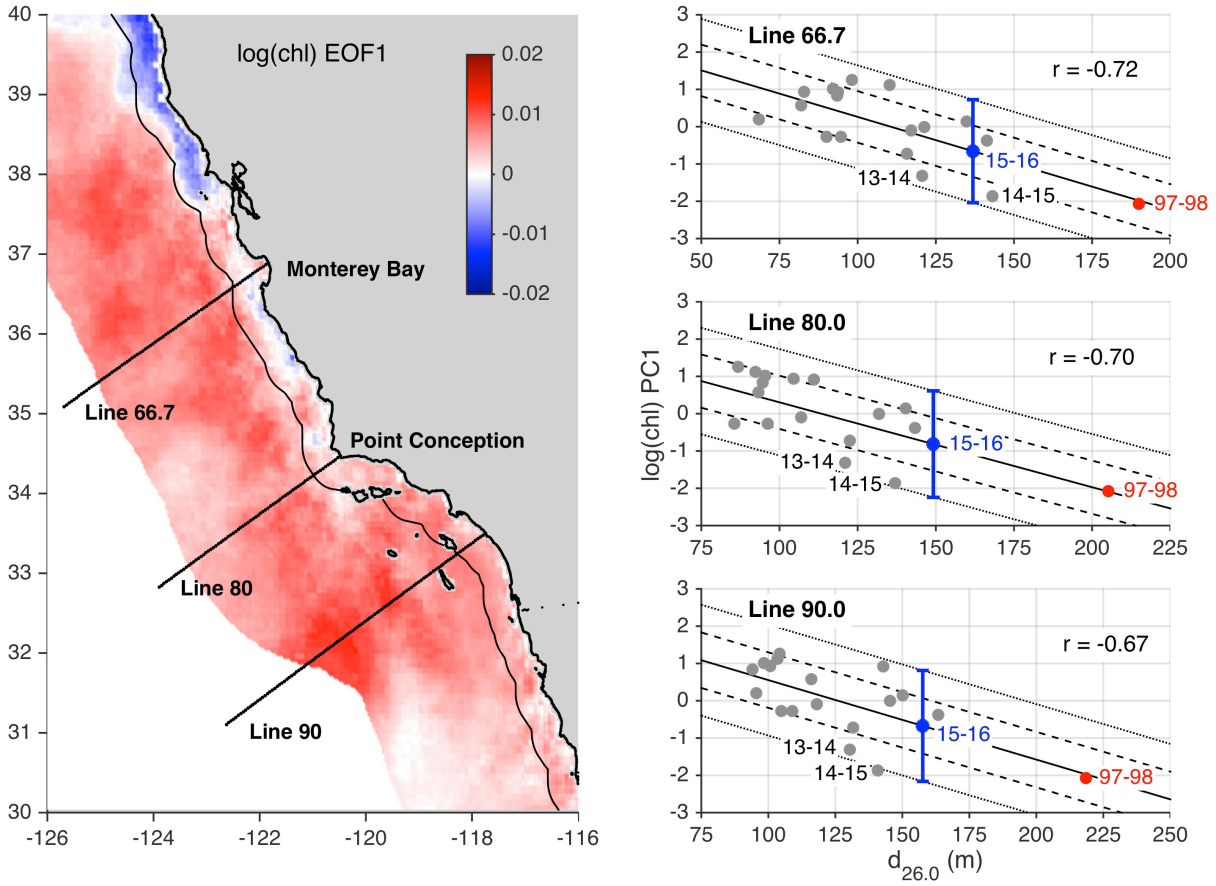

Figure 6: (left) Leading EOF of surface chlorophyll in a 300 km wide coastal band from 30 to 40˚N. Chlorophyll was log-transformed and averaged from April to July before computing EOFs. EOF1 captures 32% of the observed variance. (right) Amplitude of PC1 (corresponding to EOF1) plotted against December-February mean $d_{26.0}$, averaged within 50 km of shore along each glider line. Solid black lines are linear fits to the data, dashed and dotted lines are ±1 and ±2 standard deviations about the linear fit. Note that scatter plots describe the relationship between winter $d_{26.0}$ and chlorophyll the following spring (e.g., '97-98' is log(chl) PC1 for April-July 1998 plotted against $d_{26.0}$ for Dec. 1997-Feb. 1998). The 95% confidence intervals for spring/summer 2016 chlorophyll (blue lines) are estimated based on observed winter 2015-16 $d_{26.0}$.

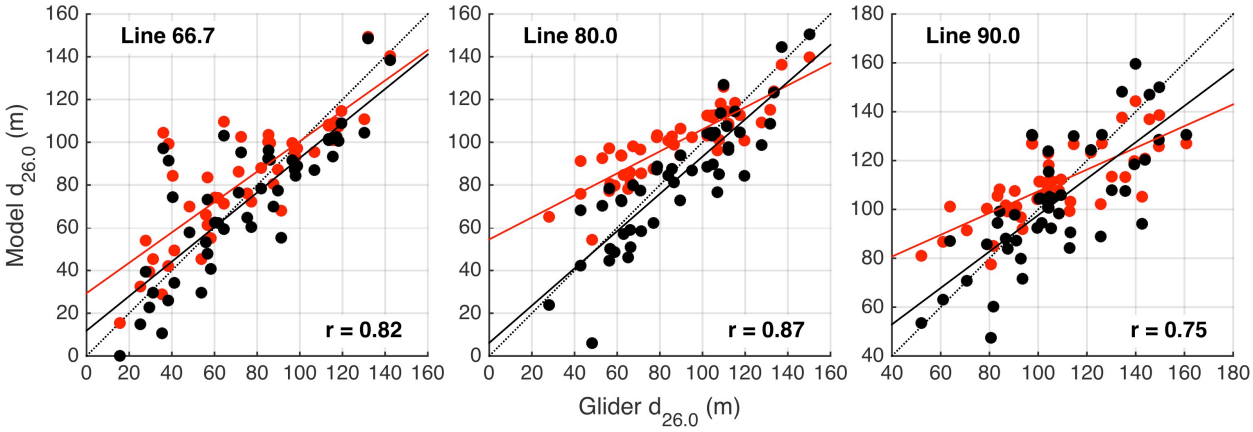

399

400 Figure S1: Comparison of monthly averaged glider and model-derived estimates of 26.0 kg m^{-3}
401 isopycnal depth, averaged within 50 km of the coast, for each glider line in the period of
402 model/glider overlap (2007-2010). Red markers show uncorrected model data while black
403 markers use bias- and variance-corrected model estimates. Solid lines are linear fits to the data;
404 dotted line is 1:1. Note that bias and variance correction does not change the correlation
405 coefficient, r.